Effective Disturbance Compensation Method Under Control Saturation in Discrete-Time Sliding Mode Control

Ji-Seok Han, *Student Member, IEEE*, Tae-Il Kim, Tae-Ho Oh, Sang-Hoon Lee, and Dong-Il "Dan" Cho, *Member, IEEE*

***Abstract*—This article presents a novel method of dealing with disturbances and control saturation in the framework of discrete-time sliding mode control (DSMC). A DSMC with decoupled disturbance compensator (DDC) was developed for SMC to recover the loss of stability in the discrete-time domain. However, windup phenomena occur in both the switching function and the disturbance estimate when control saturation occurs, and the method cannot guarantee stability. The article develops a new method for maintaining stability under both disturbances and control saturation by incorporating a novel auxiliary state into the DSMC with DDC method. The auxiliary state prevents the windup phenomena, and the developed new method preserves the asymptotic convergence property of the disturbance estimation error dynamics and the stability of the sliding mode dynamics. Also, the error states are stable under bounded disturbances and control saturation. Simulations and experiments are performed on a commonly used industrial servo system to demonstrate the effectiveness of the proposed method.**

***Index Terms*—Discrete-time systems, sliding mode control (SMC), servosystems.**

I. Introduction

SLIDING mode control (SMC) is a special kind of variable structure control and is one of the most successful approaches in general control systems with bounded and matched disturbances. SMC drives the state variables to a predesigned sliding surface in a finite time and then keeps them on the sliding surface in the presence of the bounded disturbance. Therefore, SMC exhibits invariance and finite convergence properties as well as robustness to unknowns such as external disturbances, parametric uncertainties, parameter variations, and unmodeled dynamics. In addition, it has been successfully combined with other control strategies, such as adaptive control [1], [2], backstepping control [3], and disturbance observer (DOB)-based control [4]–[9] to improve control performances or enhance its robustness against uncertainty. Super twisting control algorithms and higher order sliding mode schemes also provide excellent performance with little chattering [10]–[13]. Based on these research results, SMC has attracted attention for a wide variety of applications, such as manufacturing systems [14], robotics [15], unmanned aerial vehicles [16], and servo track writing systems [17]. In addition, there are remarkable results by applying the SMC framework to more general and complex models such as Takagi and Sugeno fuzzy systems and semi-Markovian jump systems [18]–[21].

Recently, SMC with DOB has been investigated and implemented in a variety of applications, attributed to its excellent performances of disturbance compensation. For example, an SMC method with extended sliding mode DOB has been proposed to improve the transient response of a permanent-magnet synchronous motor system [4]. An SMC method with nonlinear DOB has been developed for mismatched uncertain systems [5]. The implementation of the DOB reduced the switching gain of the discontinuous control part of SMC, which alleviated chattering. An SMC method with extended DOB has also been proposed for a general nth-order system with mismatched uncertainties [6]. This method showed accurate estimation performance in the presence of complex unmatched disturbances. An adaptive parameter estimation method and a saturation function were utilized in this controller to alleviate chattering. An integral SMC method with DOB has developed for a linear system with mismatched disturbances, and the stability was investigated using the H_∞ control and steady-state output approaches [7]. SMC-based DOBs also have been designed in an asymmetric underactuated surface vehicle and a marine vehicle, respectively [8], [9]. By exploiting finite-time convergence property of the sliding mode observers, the external disturbances and unmodeled dynamics are precisely estimated in a short time, which provides superior tracking performances.

In the discrete-time domain, however, an ideal sliding mode is not achievable due to the finite sampling period. Instead, the

Manuscript received November 18, 2018; revised March 1, 2019 and April 25, 2019; accepted June 26, 2019. Date of publication August 13, 2019; date of current version March 4, 2020. This work was supported in part by the World Class 300 Project (R&D) (S2563339) of the Ministry of SMEs and Startups (Korea). *(Corresponding author: Dong-il "Dan" Cho.)*

J. Han, T. Kim, and T. Oh are with the Department of Electrical and Computer Engineering and Automation and Systems Research Institute, Seoul National University, Seoul 08826, Korea (e-mail: jshan0803@snu.ac.kr; ehoiz@snu.ac.kr; taeho2139@snu.ac.kr).

S. Lee is with the Research and Development Center, RS Automation Company, Ltd., Pyeongtaek 17709, Korea (e-mail: shlee@rsautomation.co.kr).

D. Cho is with the Department of Electrical and Computer Engineering, Interuniversity Semiconductor Research Center, and Automation and Systems Research Institute, Seoul National University, Seoul 08826, Korea (e-mail: dicho@snu.ac.kr).

Color versions of one or more of the figures in this article are available online at http://ieeexplore.ieee.org

Digital Object Identifier 10.1109/TIE.2019.2931213

state trajectories are bounded within a small band and exhibit a zig-zag motion after the reaching mode, which is referred to as a quasi-sliding mode (QSM). Thus, the invariant properties are lost when SMC is implemented in the discrete-time domain. A discrete-time sliding mode control (DSMC) law has been proposed, which guarantees the reaching and QSMs in discrete time [22]. A new discrete reaching law has been developed, which reduces the width of QSM by using the continuous-approximation and difference functions [23]. The DSMC with DOB methods have also been analyzed. A DSMC method combined with a decoupled disturbance compensator (DDC) has been developed to recover the loss of stability for SMC in discrete-time systems [24], [25]. It can be shown that the DDC has the same structure as the conventional DOB [26], and the DSMC with DOB methods have been successfully implemented in industrial applications [27]–[29]. However, these works assumed that the control inputs are unconstrained, and they lose stability when control saturation occurs.

Control saturation dramatically degrades system performance, for example, significant overshoot, undershoot, oscillations, limit cycles, and even instability can occur. Recently, robust control schemes have been developed to deal with disturbances and control saturation. For example, an adaptive SMC method has been developed to stabilize a spacecraft with uncertainty in inertia, external disturbances, and control saturation [30]. A backpropagating constraints-based control is designed to ensure high tracking performance for a quadrotor with complex unknowns and constrained actuator dynamics [31]. Antiwindup methods are general approaches to deal with control saturation. Modern antiwindup techniques have also been researched to guarantee quadratic stability of linear control systems by formulating linear matrix inequality (LMI) [32]–[34]. However, antiwindup compensators are difficult to incorporate into a nonlinear control framework such as SMC. Robust control methods combining auxiliary states have also been researched. A backstepping control method with the nonlinear DOB and the auxiliary state has been developed to estimate the unknown external disturbances for a surface vessel [35]. Backstepping control methods combined with the auxiliary state have been proposed for an autonomous spacecraft to deal with control saturation, parametric uncertainty, and external disturbances [36]–[38]. An adaptive SMC method combined with nonlinear DOB and the auxiliary state has been proposed for autonomous underwater vehicles to deal with disturbances and control saturation [39]. However, it is derived in the continuous-time domain. A novel disturbance estimation scheme has been developed for a DSMC [40]. It prevents the windup of the disturbance estimate and, thus, guarantees the asymptotic convergence of the disturbance estimation error dynamics even in the presence of control saturation. However, there is still a limitation that windup phenomenon occurs in the switching function under control saturation, and thus the method cannot guarantee the stability of sliding mode dynamics.

This article proposes a novel DSMC with DDC method to deal with disturbances and control saturation using an auxiliary state. In specific, the closed-loop stability for a double integrator system is investigated, where the double integrator model has been applied in a wide range of practical systems [41], such as industrial servo systems [40], multiagent systems [42], [43], and autonomous underwater vehicles [44]. The main contributions of this article are as follows. First, the new auxiliary state is incorporated into the switching function of DSMC, which prevents the windup effects of both the switching function and the disturbance estimate. Therefore, the proposed method can preserve the asymptotic convergence property of the disturbance estimation error dynamics and guarantees the stability of the sliding mode dynamics in the presence of disturbances and control saturation. Second, the stability of the error dynamics is analyzed based on the existence of a quadratic Lyapunov function. Given the conditions for sector nonlinearity of the deadzone function and the boundedness of disturbances, a sufficient condition for the stability of error dynamics is formulated based on the LMI approach. Therefore, the tracking error is eventually bounded in a small region. The proposed control laws are originally expressed in the discrete-time domain, and thus a discretization process for implementation in digital controllers is not required. In addition, the boundary layer technique for the switching function is utilized to alleviate the chattering effect. Therefore, the developed method is highly applicable to many practical applications.

The rest of this article is structured as follows. Section II provides the preliminaries of DSMC with DDC and formulates the problem of the DSMC with DDC under control saturation. In Section III, the novel DSMC with DDC method using the auxiliary state is presented, and stability analysis is carried out. Section VI studies the simulations for the DSMC with DDC and auxiliary state under disturbances and control saturation in detail. Finally, Section V demonstrates experimental results performed on an industrial ball-screw drive system, and Section VI concludes this article.

II. Preliminaries and Problem Formulation

A. Problem Formulations With Unconstrained Control Input

Consider the following double integrator system in the discrete-time domain with an unconstrained input and a matched disturbance:

$$\mathbf{x}_{k+1} = \mathbf{A}\mathbf{x}_k + \mathbf{B}u_k + \mathbf{B}f_k \tag{1}$$

where $\mathbf{x}_k \in \mathbb{R}^2$ is the state vector, $u_k \in \mathbb{R}$ is the unconstrained control input, $\mathbf{A} = \left[\begin{smallmatrix} 1 & T \\ 0 & 1 \end{smallmatrix}\right]$ is the system matrix, $\mathbf{B} = \left[\begin{smallmatrix} cT^2/2 \\ cT \end{smallmatrix}\right]$ is the input matrix, c is the model parameter, and $f_k \in \mathbb{R}$ is the matched disturbance. The disturbance contains all unknown inputs that come from external disturbances, parametric uncertainties, parameter variations, and unmodeled dynamics. The following assumption holds through this article.

Assumption 1: The changing rate of the disturbance f_k is bounded by some non-negative constant m, i.e., $|f_k - f_{k-1}| \leq m$. It means that the disturbance is sufficiently slowly varying.

The switching function is designed as follows:

$$s_k = \mathbf{G}\mathbf{e}_k = \mathbf{G}\left(\mathbf{x}_k - \mathbf{x}_k^{\text{ref}}\right) \tag{2}$$

where $\mathbf{e}_k \in \mathbb{R}^2$ is the error vector and defined as $\mathbf{e}_k = \mathbf{x}_k - \mathbf{x}_k^{\text{ref}}$, $\mathbf{x}_k^{\text{ref}} \in \mathbb{R}^2$ is the reference vector, and $\mathbf{G} = [\, g_1 \;\; g_2 \,] \in \mathbb{R}^2$ is the row vector that determines the slope of the sliding manifold. For (1), the DSMC with DDC law is given by

$$u_k = -\hat{f}_k + (\mathbf{GB})^{-1}\left[\mathbf{G}\mathbf{x}_{k+1}^{\text{ref}} - \mathbf{GA}\mathbf{x}_k + qs_k - \eta\,\text{sat}\left(\frac{s_k}{\phi}\right)\right] \tag{3}$$

$$\hat{f}_k = \hat{f}_{k-1} + g(\mathbf{GB})^{-1}\left[s_k - qs_{k-1} + \eta\,\text{sat}\left(\frac{s_{k-1}}{\phi}\right)\right] \tag{4}$$

where q is the parameter that determines the reaching speed to the sliding manifold, η is the switching gain of the discontinuous control, 2ϕ is the boundary layer thickness of the saturation function, $\hat{f}_k$ is the estimated disturbance, and g is the gain of the DDC. The saturation function $\text{sat}(\cdot)$ is defined as

$$\text{sat}\,(u_k) = \begin{cases} \frac{u_k}{|u_k|} & \text{if } |u| > 1 \\ u_k & \text{otherwise} \end{cases}. \tag{5}$$

For (1) with (3) and (4), the sliding mode dynamics and the disturbance estimation error dynamics are satisfied as follows:

$$s_{k+1} = qs_k - \eta\text{sat}\left(\frac{s_k}{\phi}\right) + \mathbf{GB}\tilde{f}_k \tag{6}$$

$$\tilde{f}_{k+1} = (1-g)\,\tilde{f}_k + f_{k+1} - f_k \tag{7}$$

where $\tilde{f}_k$ is the disturbance estimation error and is defined as follows:

$$\tilde{f}_k = f_k - \hat{f}_k. \tag{8}$$

Equations (6) and (7) are the key dynamics of the DSMC with DDC. The performance of the DSMC with DDC can be enhanced by increasing $g_1/g_2, 1-q, \eta$, and g. Consider the system described by (1) with Assumption 1 and control parameters that satisfy $0 < \eta/\phi < q < 1$, $0 < g < 1$ and $\eta > \mathbf{GB}(m/g)$. If the disturbance estimation law is chosen as (4), the disturbance estimation error is ultimately bounded by m/g, i.e., $|\tilde{f}_k| < m/g$ for $k \geq k'$ where k' is a positive integer. In addition, if the control law is chosen as (3), the sliding mode dynamics (6) are stable. Rigorous proofs of these claims are given in [24]. However, in practice, the magnitude of the control input is limited, so neither (6) nor (7) is satisfied under control saturation, which is discussed in the following subsection.

B. Problem Formulations With Constrained Control Input

Consider the following constrained input system:

$$\mathbf{x}_{k+1} = \mathbf{A}\mathbf{x}_k + \mathbf{B}u^{\text{lim}}\,\text{sat}\left(\frac{u_k}{u^{\text{lim}}}\right) + \mathbf{B}f_k \tag{9}$$

where u^{lim} is the positive limit of the control input. The saturation nonlinearity in (9) can be expressed in terms of the deadzone nonlinearity as follows:

$$\mathbf{x}_{k+1} = \mathbf{A}\mathbf{x}_k + \mathbf{B}u_k - \mathbf{B}q_k + \mathbf{B}f_k \tag{10}$$

$$q_k = dz\,(u_k) = u_k - u^{\text{lim}}\,\text{sat}\left(\frac{u_k}{u^{\text{lim}}}\right) \tag{11}$$

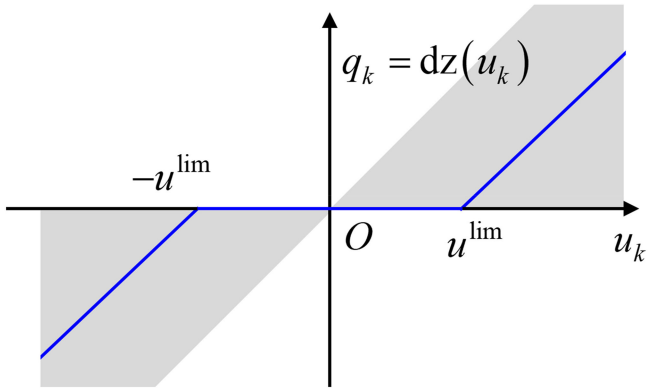

Fig. 1. Deadzone function.

where $\text{dz}(\cdot)$ is the deadzone function. The graphical representation of $\text{dz}(\cdot)$ is depicted in Fig. 1. If the control methods (3) and (4) are used, then the disturbance estimation error dynamics are derived as follows:

$$\tilde{f}_k = (1-g)\,\tilde{f}_{k-1} + f_k - f_{k-1} + gq_{k-1}. \tag{12}$$

Comparing (12) with (7), the disturbance estimation error dynamics include the additional term gq_{k-1}. Generally, the nature of q_k is abrupt and unpredictable. Thus, $\tilde{f}_k$ may not converge asymptotically when control saturation arises. To guarantee the asymptotic convergence of the disturbance estimation error dynamics under control saturation, a new disturbance estimation method was developed [40]. For (9) with Assumption 1, consider the DSMC law (3) and the following disturbance estimation law with control parameters that satisfy $0 < \eta/\phi < q < 1$, $0 < g < 1$ and $\eta > \mathbf{GB}(m/g)$:

$$\begin{aligned}\hat{f}_k = {} & (1-g)\hat{f}_{k-1} + g(\mathbf{GB})^{-1} \\ & \times \mathbf{G}(\mathbf{x}_k - \mathbf{A}\mathbf{x}_{k-1} - \mathbf{B}u_{k-1} + \mathbf{B}q_{k-1}).\end{aligned} \tag{13}$$

Then, the disturbance estimation error dynamics of the DSMC with DDC will converge asymptotically even if control saturation occurs. The disturbance estimation error dynamics are given by

$$\tilde{f}_k = (1-g)\,\tilde{f}_{k-1} + f_k - f_{k-1} \tag{14}$$

which is equal to (7). The validity and effectiveness of the disturbance compensator (13) were also demonstrated with experimental results [40]. However, the stability of the sliding mode dynamics are not guaranteed as follows:

$$\begin{aligned} s_{k+1} &= \mathbf{G}\mathbf{e}_{k+1} = \mathbf{G}\left(\mathbf{x}_{k+1} - \mathbf{x}_{k+1}^{\text{ref}}\right) \\ &= \mathbf{G}\left(\mathbf{A}\mathbf{x}_k + \mathbf{B}u_k - \mathbf{B}q_k + \mathbf{B}f_k\right) - \mathbf{G}\mathbf{x}_{k+1}^{\text{ref}} \\ &= \mathbf{GA}\mathbf{x}_k - \mathbf{GB}\hat{f}_k \\ &\quad + \left(\mathbf{G}\mathbf{x}_{k+1}^{\text{ref}} - \mathbf{GA}\mathbf{x}_k + qs_k - \eta\text{sat}\left(\frac{s_k}{\phi}\right)\right) \\ &\quad - \mathbf{GB}q_k + \mathbf{GB}f_k - \mathbf{G}\mathbf{x}_{k+1}^{\text{ref}} \\ &= qs_k - \eta\text{sat}\left(\frac{s_k}{\phi}\right) + \mathbf{GB}\tilde{f}_k - \mathbf{GB}q_k. \end{aligned} \tag{15}$$

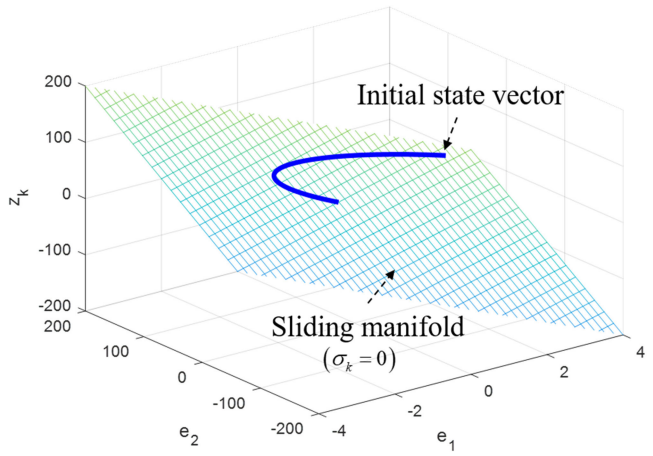

Fig. 2. State trajectory of DSMC with DDC and auxiliary state.

Due to the remaining term $\mathbf{GB}q_k$ in (15), which is abrupt and unpredictable, the windup phenomenon of the switching function arises. Therefore, there is a possibility of undesirable effects, such as transient overshoot, undershoot, oscillations, limit cycles, and instability.

III. Proposed Method

In this section, a novel DSMC method for dealing with disturbances and control saturation is presented. For the system (9), the following auxiliary dynamics are newly introduced as follows:

$$z_k = \alpha z_{k-1} + (\mathbf{GB})\, q_{k-1} \tag{16}$$

where $z_k \in \mathbb{R}$ is the auxiliary state, and $0 < \alpha < 1$ is the gain of auxiliary dynamics (16). A novel switching function, $\sigma_k \in \mathbb{R}$, is defined as follows:

$$\sigma_k := \mathbf{G}\mathbf{e}_k + z_k. \tag{17}$$

Note that the auxiliary state is incorporated into the switching function, which is the main idea of this article. Using (16) and (17), the new control and disturbance estimation laws are developed as follows:

$$u_k = -\hat{f}_k + (\mathbf{GB})^{-1} \times \left(\mathbf{G}\mathbf{x}_{k+1}^{\text{ref}} - \mathbf{G}\mathbf{A}\mathbf{x}_k - \alpha z_k + q\sigma_k - \eta \text{sat}\left(\frac{\sigma_k}{\phi}\right)\right) \tag{18}$$

$$\hat{f}_k = \hat{f}_{k-1} + g(\mathbf{GB})^{-1}\left[\sigma_k - q\sigma_{k-1} + \eta \text{sat}\left(\frac{\sigma_{k-1}}{\phi}\right)\right]. \tag{19}$$

Using the auxiliary state, the dimension of the sliding hyperplane increases by one. Fig. 2 shows an example of a state trajectory with the proposed control method. The proposed auxiliary state plays a significant role for the DSMC with DDC structure under control saturation. When the control saturation arises, the auxiliary state stores the amount of windup for the switching function with the decaying rate of α. Therefore, the sliding mode is always guaranteed to be stable under disturbances and control saturation which is discussed in the following theorem.

Theorem 1: Consider the constrained input system (9) with Assumption 1. The auxiliary state and the switching function are defined as (16) and (17), respectively. If the control law (18) and disturbance estimation law (19) are chosen as with control parameters that satisfy $0 < \eta/\phi < q < 1$, $0 < g < 1$, and $\eta > \mathbf{GB}(m/g)$, then the sliding mode dynamics and the disturbance estimation error dynamics are satisfied as follows:

$$\sigma_{k+1} = q\sigma_k - \eta \text{sat}\left(\frac{\sigma_k}{\phi}\right) + \mathbf{GB}\tilde{f}_k \tag{20}$$

$$\tilde{f}_{k+1} = (1-g)\,\tilde{f}_k + f_{k+1} - f_k. \tag{21}$$

Proof: By substituting (9) and (18) into (17), (20) is easily obtained as

$$\begin{aligned}
\sigma_{k+1} &= \mathbf{G}\left(\mathbf{x}_{k+1} - \mathbf{x}_{k+1}^{\text{ref}}\right) + z_{k+1} \\
&= \mathbf{G}\mathbf{A}\mathbf{x}_k + \mathbf{G}\mathbf{B}u_k - \mathbf{G}\mathbf{B}q_k \\
&\quad + \mathbf{G}\mathbf{B}f_k - \mathbf{G}\mathbf{x}_{k+1}^{\text{ref}} + \alpha z_k + \mathbf{G}\mathbf{B}q_k \\
&= \mathbf{G}\mathbf{A}\mathbf{x}_k - \mathbf{G}\mathbf{B}\hat{f}_k + \mathbf{G}\mathbf{x}_{k+1}^{\text{ref}} \\
&\quad - \mathbf{G}\mathbf{A}\mathbf{x}_k - \alpha z_k + q\sigma_k - \eta \text{sat}\left(\frac{\sigma_k}{\phi}\right) \\
&\quad + \mathbf{G}\mathbf{B}f_k - \mathbf{G}\mathbf{x}_{k+1}^{\text{ref}} + \alpha z_k \\
&= q\sigma_k - \eta \text{sat}\left(\frac{\sigma_k}{\phi}\right) + \mathbf{G}\mathbf{B}\tilde{f}_k.
\end{aligned} \tag{22}$$

From (22), the following equation holds:

$$\tilde{f}_{k-1} = (\mathbf{GB})^{-1}\left(\sigma_k - q\sigma_{k-1} + \eta \text{sat}\left(\frac{\sigma_{k-1}}{\phi}\right)\right). \tag{23}$$

Substituting (23) into (19), the disturbance estimation law is written as follows:

$$\begin{aligned}
\hat{f}_k &= \hat{f}_{k-1} + g\tilde{f}_{k-1} \\
&= (1-g)\,\hat{f}_{k-1} + g f_{k-1}.
\end{aligned} \tag{24}$$

With (8) and (24), the disturbance estimation error dynamics are derived as follows:

$$\begin{aligned}
\tilde{f}_k &= f_k - \hat{f}_k \\
&= f_k - (1-g)\,\hat{f}_{k-1} - g f_{k-1} + f_{k-1} - f_{k-1} \\
&= (1-g)\,\tilde{f}_{k-1} + f_k - f_{k-1}
\end{aligned} \tag{25}$$

which is the same as (21). ■

The two equations in (20) and (21) are the key dynamics in this article. The two dynamics are always satisfied even in the presence of disturbances and control saturation. The following lemma provides the ultimate boundedness of the disturbance estimation error dynamics.

Lemma 1: For a system (9), if Assumption 1 holds and $0 < g < 1$, the disturbance estimation error is ultimately bounded by m/g, i.e., $|\tilde{f}_k| < m/g$ for $k \geq k'$ where k' is a positive integer. In addition, for a constant disturbance, the disturbance estimation error asymptotically converges to zero.

Proof: Consider the following scalar discrete dynamical system:

$$v_k = (1-g)\, v_{k-1} + m \tag{26}$$

where v_k is a convergent sequence with $v_0 = \tilde{f}_0$. Obviously, (26) can be written as follows:

$$v_k = (1-g)^k \,(v_0 - m/g) + m/g. \tag{27}$$

Thus, v_k approaches m/g. Similarly, consider another scalar discrete dynamical system

$$w_k = (1-g)\, w_{k-1} - m \tag{28}$$

where w_k is a convergent sequence with $w_0 = \tilde{f}_0$. Thus, w_k approaches $-m/g$. By using the comparison lemma [45], $\tilde{f}_k$ is sandwiched between v_k and w_k. Therefore, the absolute value of the disturbance estimation error is ultimately bounded by m/g. In addition, for a constant disturbance, i.e., $m = 0$, the disturbance estimation error asymptotically converges to zero. ■

Remark 1: The disturbance estimation error dynamics depend only on the parameter g, so the disturbance estimation performance can be tuned by adjusting the parameter of g. This decoupling property explains why (19) is referred to as a DDC. The analysis for selecting the values of g will be discussed in Section VI.

The following theorem guarantees the stability of sliding mode dynamics in DSMC with DDC by utilizing the auxiliary state under disturbances and control saturation.

Theorem 2: For system (9) with Assumption 1 and controllers as Theorem 1, the states enter into the small region, i.e., $|\sigma_k| < \frac{\mathbf{GB}(m/g)}{1-q+\eta/\phi}$, where $\frac{\mathbf{GB}(m/g)}{1-q+\eta/\phi} < \phi$. It means that the sliding mode dynamics are always guaranteed under disturbances and control saturation.

Proof: The strict condition for Lyapunov stability of the DSMC with DDC will be verified based on the comparison lemma [45]. Consider the case $\sigma_k > \phi$. Then σ_k is upper-bounded by σ'_k whose dynamics are given by

$$\sigma'_{k+1} = q\sigma'_k - \eta + \mathbf{GB}\,(m/g) \tag{29}$$

where $\sigma'_0 = \sigma_0$. Thus, σ'_k can be represented by the following sequence:

$$\sigma'_k = q^k \left(\sigma'_0 - \frac{\mathbf{GB}\,(m/g) - \eta}{1-q}\right) + \frac{\mathbf{GB}\,(m/g) - \eta}{1-q}. \tag{30}$$

It can easily check that σ'_k converges to $\frac{\mathbf{GB}(m/g)-\eta}{1-q}$, which is less than zero. Therefore, σ_k eventually enters in $|\sigma_k| < \phi$. In the same way, when $\sigma_k < -\phi$, σ_k enters in $|\sigma_k| < \phi$. Finally, when $|\sigma_k| \le \phi$, σ_k is sandwiched between the following two sequences:

$$\sigma''_k = q^k \left(\sigma''_0 - \frac{\mathbf{GB}\,(m/g)}{1-q+\frac{\eta}{\phi}}\right) + \frac{\mathbf{GB}\,(m/g)}{1-q+\frac{\eta}{\phi}} \tag{31}$$

$$\sigma'''_k = q^k \left(\sigma'''_0 + \frac{\mathbf{GB}\,(m/g)}{1-q+\frac{\eta}{\phi}}\right) - \frac{\mathbf{GB}\,(m/g)}{1-q+\frac{\eta}{\phi}} \tag{32}$$

where $\sigma''_0 = \sigma'''_0 = \sigma_0$. Therefore, σ_k eventually enters in $|\sigma_k| < \frac{\mathbf{GB}(m/g)}{1-q+\eta/\phi}$. Note that $\frac{\mathbf{GB}(m/g)}{1-q+\eta/\phi} < \phi$ by using the following inequalities:

$$\mathbf{GB}\,(m/g) < \eta + \phi\,(1-q)\,. \tag{33}$$

By dividing both sides of (33) by $1-q+\eta/\phi$ which is larger than zero, the inequality $\frac{\mathbf{GB}(m/g)}{1-q+\eta/\phi} < \phi$ holds. Therefore, the sliding mode dynamics are stable. ■

Remark 2: When α is closer to one, the auxiliary dynamics will be slower. In that case, the closed-loop response of the DSMC with DDC under control saturation is smoother. However, the dynamics of the auxiliary state will be dominant, and the response will be slow. Therefore, the tradeoff relationship needs to be considered.

Assumption 2: The peak of f_k is bounded by $M \ge 0$, which is smaller than $u^{\lim}$, i.e., $|f_k| \le M < u^{\lim}$.

Assumption 3: Under control saturation, the reference model satisfies the following equation in finite time:

$$\mathbf{x}^{\mathrm{ref}}_{k+1} = \mathbf{A}\mathbf{x}^{\mathrm{ref}}_k. \tag{34}$$

Remark 3: Assumption 2 is a trivial condition in practice. For example, if the maximum control limit is less than the amplitude of disturbance, any control method does not guarantee stability or the desired performance. Therefore, the maximum control limit should be sufficiently large against the peak of disturbance. In physical systems, such as servo systems with gravity or friction effects, the bounded-peak condition for disturbance is very common compared to the bounded-energy condition. Assumption 3 is rather constrained, but it is admissible in general robust tracking control system [46], [47]. For these applications, control saturation generally arises when the reference profile is given with high acceleration. Thus, the acceleration component of the reference model should be restricted in a finite time to stabilize the system. Therefore, the velocity of the reference is assumed to be constant under control saturation, so that the reference model can be represented as (34).

Remark 4: When control saturation does not arise, the control law (18) and the disturbance estimation law (19) are the same as the original DSMC law (3) and the DDC law (4), respectively. The auxiliary state activates only under control saturation, and, thus, the additional dynamics do not occur when the control input is not saturated and the initial value of the auxiliary state is zero. Therefore, the asymptotic convergence property of the disturbance estimation error dynamics and the closed-loop stability proposed in [24] are preserved in the presence of control saturation.

The next theorem provides the robust stability of the error dynamics for the proposed method under disturbances and control saturation.

Theorem 3: For (9) with Assumptions 1–3, the proposed methods (16)–(19) are used. Suppose that $|\sigma_k| < \phi$ is based on Theorem 2. Then the error states are stable and ultimately bounded by an ellipsoid region. In addition, for a constant disturbance, the error states converge asymptotically to zero.

Proof: In the boundary layer, the control input is given by

$$\begin{aligned} u_k &= -\hat{f}_k + (\mathbf{GB})^{-1} \\ &\quad \times \left(\mathbf{G}\mathbf{x}_{k+1}^{\text{ref}} - \mathbf{GAx}_k - \alpha z_k + \left(q - \frac{\eta}{\phi}\right)\sigma_k \right) \\ &= -\hat{f}_k - (\mathbf{GB})^{-1} \\ &\quad \times \left(\mathbf{GAe}_k + \alpha z_k - \left(q - \frac{\eta}{\phi}\right)(\mathbf{Ge}_k + z_k) \right) \\ &= -\hat{f}_k - (\mathbf{GB})^{-1}\mathbf{G} \\ &\quad \times \left(\mathbf{A} - \left(q - \frac{\eta}{\phi}\right)\mathbf{I} \right) \mathbf{e}_k - (\mathbf{GB})^{-1}\left(\alpha - q + \frac{\eta}{\phi}\right) z_k \\ &= -\hat{f}_k - \mathbf{Ke}_k - \delta z_k \end{aligned} \tag{35}$$

where $\mathbf{K} = [\,k_1 \;\; k_2\,] = (\mathbf{GB})^{-1}\mathbf{G}(\mathbf{A} - (q - \frac{\eta}{\phi})\mathbf{I})$

$$\delta = (\mathbf{GB})^{-1}\left(\alpha - q + \frac{\eta}{\phi}\right).$$

Using (9) and (35) with Assumption 3, the error dynamics can be represented as follows:

$$\mathbf{e}_{k+1} = (\mathbf{A} - \mathbf{BK})\,\mathbf{e}_k - \delta\mathbf{B}z_k - \mathbf{B}q_k + \mathbf{B}\tilde{f}_k. \tag{36}$$

With (16), (24), and (36), the following closed-loop system of DSMC with DDC and auxiliary state can be formulated:

$$\begin{aligned} \mathbf{w}_{k+1} &= \mathbf{\Phi}\mathbf{w}_k + \mathbf{\Gamma}_1 q_k + \mathbf{\Gamma}_2 f_k \\ u_k &= -\mathbf{H}\mathbf{w}_k \\ y_k &= \mathbf{C}\mathbf{w}_k \end{aligned} \tag{37}$$

where $\mathbf{w}_k = \begin{bmatrix} \mathbf{e}_k \\ \hat{f}_k \\ z_k \end{bmatrix}$, $\mathbf{\Phi} = \begin{bmatrix} \mathbf{A} - \mathbf{BK} & -\mathbf{B} & -\delta\mathbf{B} \\ \mathbf{0}_{1\times 2} & 1 - g & 0 \\ \mathbf{0}_{1\times 2} & 0 & \alpha \end{bmatrix}$

$$\mathbf{\Gamma}_1 = \begin{bmatrix} -\mathbf{B} \\ 0 \\ \mathbf{GB} \end{bmatrix}, \mathbf{\Gamma}_1 = \begin{bmatrix} \mathbf{B} \\ g \\ 0 \end{bmatrix}, \mathbf{H} = \begin{bmatrix} \mathbf{K} \; 1 \; \delta \end{bmatrix}, \mathbf{C} = \begin{bmatrix} 1 & \mathbf{0}_{1\times 3} \end{bmatrix}.$$

The dimensions of $\mathbf{w}_k, \mathbf{\Phi}, \mathbf{\Gamma}_1, \mathbf{\Gamma}_2, \mathbf{H},$, and $\mathbf{C}$ are appropriately defined. In this case, the performance output of (37) is defined as the first entry of $\mathbf{w}_k$. The closed-loop system (37) can be depicted in Fig. 3.

To guarantee the Lyapunov stability for (37), three conditions should be considered; first, the difference between $V(\mathbf{w}_{k+1})$ and $V(\mathbf{w}_k)$ should be negative, i.e., $\Delta V(\mathbf{w}_k) = V(\mathbf{w}_{k+1}) - V(\mathbf{w}_k) < 0$ for $\forall k$. Second, the magnitude of disturbance input should be restricted because the region where the states remain including the origin depends on the maximum value of the disturbance input. As the upper bound of the disturbance M is smaller, the area of the region is smaller. The following definitions will be useful to express the region.

Definition 1 (Reachable set with bounded-peak input, $\Re$): The set of all states that are visited by any trajectories that start from the origin with bounded-peak input

$$\Re = \left\{ \mathbf{w}_k \in \mathrm{R}^4 | \mathbf{w}_k \text{ and } f_k \text{ satisfy (37)}, \mathbf{w}_0 = \mathbf{0},\; f_k^2 \le M^2 \right\}. \tag{38}$$

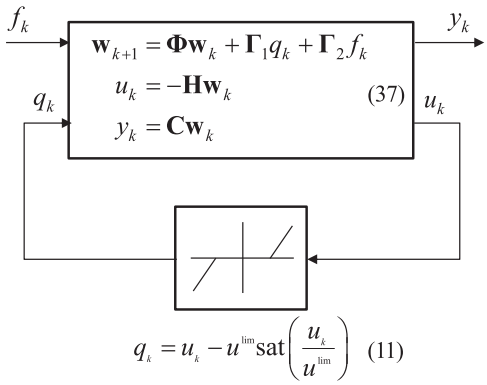

Fig. 3. Closed-loop system of DSMC with DDC and auxiliary state.

Definition 2 (Ellipsoid, E*):* The set that satisfies

$$\mathrm{E} = \left\{ \mathbf{w}_k \in \mathbb{R}^4 | \mathbf{w}_k^T \mathbf{Q} \mathbf{w}_k \le 1 \right\}. \tag{39}$$

Lemma 2 [48]*:* Suppose that there exists a quadratic function $V(\mathbf{w}_k) = \mathbf{w}_k^T \mathbf{Q} \mathbf{w}_k$ where $\mathbf{Q} \in \mathbb{R}^{4\times 4}$ is symmetric and positive definite, and $\Delta V(\mathbf{w}_k) < 0$ for all $\mathbf{w}_k$ and f_k satisfying (37), $f_k^2 \le M^2$ and $V(\mathbf{w}_k) \ge 1$. Then the ellipsoid given in (39) contains the reachable set $\Re$.

The proof of Lemma 2 is given at the end of this section. By Definition 1, the states can reach out at most the boundary of $\Re$. In that case, the set $\Re$ can be bounded by the ellipsoid E by Lemma 2. Then the following inequality can be formulated for the bounded-peak condition:

$$\tau \mathbf{w}_k^T \mathbf{P} \mathbf{w}_k - \tau M^2 f_k^2 \ge 0 \tag{40}$$

where τ is an arbitrarily positive constant. Although the initial condition of $\mathbf{w}_k$ is not zero in practice, the states will be ultimately bounded by the ellipsoid E. Last, the sector condition of the deadzone function should be considered. For the deadzone function, multiplication of the input and output always yields the following inequality:

$$2q_k\left(-\mathrm{H}\mathbf{w}_k - q_k\right) \ge 0. \tag{41}$$

In summary, by synthesizing the three conditions and applying S-procedure [48], the following sufficient condition is derived for the closed-loop stability:

$$\Delta V\left(\mathbf{w}_k\right) + 2q_k\left(-\mathbf{H}\mathbf{w}_k - q_k\right) + \tau \mathbf{w}_k^T \mathbf{P} \mathbf{w}_k - \tau M^2 f_k^2 < 0. \tag{42}$$

Thus, if a positive and symmetric matrix $\mathbf{P}$ that satisfies the following LMI exists, then the Lyapunov stability for (37) is guaranteed

$$\begin{aligned} &\mathbf{P} > 0 \\ &\begin{bmatrix} \mathbf{\Phi}^{\mathrm{T}}\mathbf{P}\mathbf{\Phi} - \mathbf{P} + \tau\mathbf{P} & \mathbf{\Phi}^{\mathrm{T}}\mathbf{P}\mathbf{\Gamma}_1 - \mathbf{H}^{\mathrm{T}} & \mathbf{\Phi}^{\mathrm{T}}\mathbf{P}\mathbf{\Gamma}_2 \\ * & \mathbf{\Gamma}_1^{\mathrm{T}}\mathbf{P}\mathbf{\Gamma}_1 - 2 & \mathbf{\Gamma}_1^{\mathrm{T}}\mathbf{P}\mathbf{\Gamma}_2 \\ * & * & \mathbf{\Gamma}_2^{\mathrm{T}}\mathbf{P}\mathbf{\Gamma}_2 - \tau M^2 \end{bmatrix} < 0 \end{aligned} \tag{43}$$

where the matrices denoted by $*$ are the transposes of the entries above the diagonal. Therefore, the error states are ultimately bounded by a small region, so the Lyapunov stability holds for (37). In addition, for a constant disturbance, the disturbance

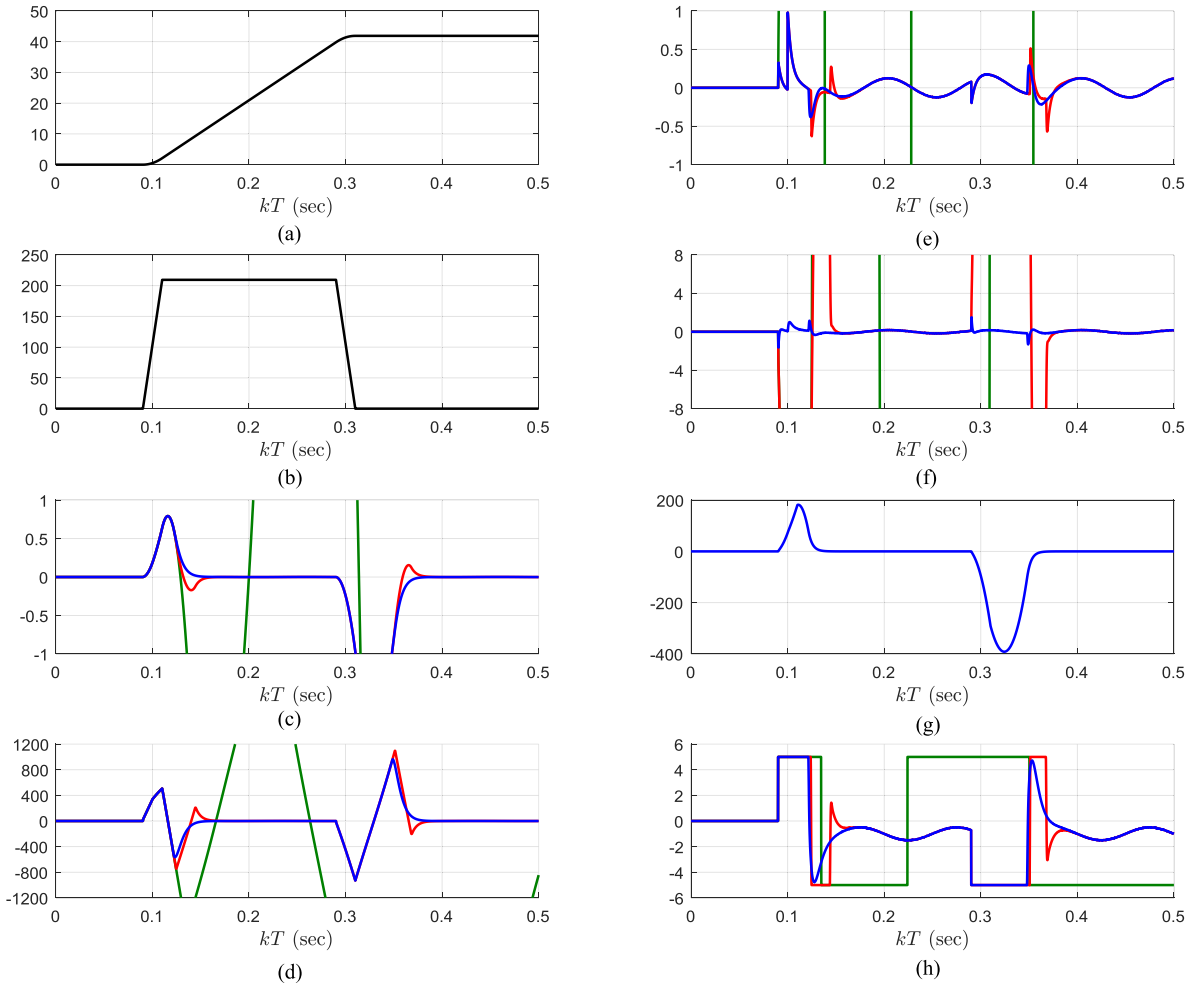

Fig. 4. Simulation results (green line: Method 1, red line: Method 2, and blue line: Method 3). (a) $x_{1,k}^{\mathrm{ref}}$. (b) $x_{2,k}^{\mathrm{ref}}$. (c) $e_{1,k}$. (d) $e_{2,k}$. (e) Disturbance estimation error $(\tilde{f}_k)$. (f) Switching function (s_k). (g) Auxiliary state (z_k). (h) Control input (u_k).

estimation error goes to zero by Lemma 1. In the same manner, the LMI using (16), (36), and (41) with $\tilde{f}_k = 0$ can be formulated again. Then the global asymptotic stability of $\mathbf{e}_k$ and z_k can be achieved. Therefore, the error states are asymptotically stable. ■

Proof of Lemma 2: If the initial states lie on the outside of ellipsoid E, then the states enter into the ellipsoid even with $f_k^2 \leq M^2$, and they cannot escape from E. Therefore, the reachable set can be estimated by considering the conditions for $f_k^2 \leq M^2$ and $V(\mathbf{w}_k) \geq 1$. ■

IV. Simulation Examples

Consider the following double integrator system with matched disturbance:

$$\begin{bmatrix} x_{1,k+1} \\ x_{2,k+1} \end{bmatrix} = \begin{bmatrix} 1 & T \\ 0 & 1 \end{bmatrix} \begin{bmatrix} x_{1,k} \\ x_{2,k} \end{bmatrix} + 1420 \begin{bmatrix} \frac{T^2}{2} \\ T \end{bmatrix} \left(5 \cdot \mathrm{sat}\left(\frac{u_k}{5} \right) + f_k \right) \tag{44}$$

where $T = 0.125$ ms. The disturbance model is given as follows:

$$f_k = \begin{cases} 0 & 0 \leq kT < 0.1 \text{ s} \\ 1 + 0.5\sin\left(2\pi \cdot 10 \cdot kT\right) & kT \geq 0.1 \text{ s} \end{cases}. \tag{45}$$

TABLE I
Gain Parameters for Simulation and Experimental Results

Parameters	$\mathbf{G}$	q	η	ϕ	g	α
Values	$\begin{bmatrix} 200 & 1 \end{bmatrix}$	0.9	0.3	10	0.03	0.97

The reference model is given as follows:

$$\begin{bmatrix} x_{1,k+1}^{\mathrm{ref}} \\ x_{2,k+1}^{\mathrm{ref}} \end{bmatrix} = \begin{bmatrix} 1 & T \\ 0 & 1 \end{bmatrix} \begin{bmatrix} x_{1,k}^{\mathrm{ref}} \\ x_{2,k}^{\mathrm{ref}} \end{bmatrix} + \begin{bmatrix} \frac{cT^2}{2} \\ cT \end{bmatrix} u_k^{\mathrm{ref}}. \tag{46}$$

The reference profile is depicted in Fig. 4(a) and (b). The error states are defined as $e_{1,k} = x_{1,k} - x_{1,k}^{\mathrm{ref}}$ and $e_{2,k} = x_{2,k} - x_{2,k}^{\mathrm{ref}}$, respectively. To compare the proposed controller over the existing methods, both the original DSMC with DDC [24] and the DSMC with DDC in [40] are tested. The terms of three control methods, i.e., the original DSMC with DDC method [24], the DSMC with DDC [40], and the proposed DSMC with DDC and auxiliary state method are referred as Method 1, Method 2, and Method 3, respectively. The parameters of the three methods are equally applied and given in Table I. In this case, the positive

and symmetric matrix P exists and can be calculated by the LMI control toolbox solver in MATLAB. The calculation result is as follows:

$$\mathbf{P} = \begin{bmatrix} 669.1610 & 139.4721 & 5.6514 & -5.0376 \\ 139.4721 & 14.9606 & 1.1369 & -8.2392 \\ 5.6514 & 1.1369 & 30.9570 & -0.4992 \\ -5.0376 & -8.2392 & -0.4992 & 52.9190 \end{bmatrix} \quad (47)$$

where τ is selected as one. In Fig. 4(e), the disturbance estimation error of Method 1 diverges due to the saturation effect. On the other hand, the disturbance estimation errors of Method 2 and Method 3 do not diverge. Also, Method 1 and 2 almost compensate for the constant component of disturbance with short transients. In addition, they reduce the 10-Hz component of disturbance by 25% in the steady state. In Fig. 4(f), the switching function of Method 1 diverges under control saturation due to the windup of both the estimated disturbance and the switching function as explained in (12) and (15). The switching function of Method 2 converges to zero in the steady state but has a quite large value due to the windup of the switching function, which leads to large values of the error states, as explained in (15). On the other hand, the switching function of Method 3 is bounded by a very small region because the auxiliary state contains the amount of windup for switching function and replaces the error dynamics of (36) with slower dynamics, which is the fundamental role of the auxiliary state. Therefore, the sliding mode dynamics are always stable as explained in (20). Fig. 4(g) shows the values of the auxiliary state for Method 3. The auxiliary state eventually converges to zero with the condition of $0 \leq \alpha < 1$. Fig. 4(h), Method 3 has the smallest time interval in control saturation and has the smoothest control input. Finally, the error states are given in Fig. 4(c) and (d). The first peaks of $e_{1,k}$ and $e_{2,k}$ occur for three. After the acceleration component of the reference satisfies Assumption 2, i.e., in the constant velocity region of the reference, Method 3 shows a superior tracking performance compared to the other methods without the second peak in the position error. In conclusion, the auxiliary state for Method 3 preserves the fundamental dynamics, i.e., (20) and (21), under disturbances and control saturation. Therefore, the tracking performance of Method 3 exhibits the most desirable performance under disturbances and control saturation.

Remark 5: If the parameter g is increased, the peak value of disturbance estimation error decreases. Fig. 5 shows the comparison results for the disturbance estimation error with different gains of g by using Method 3. In the steady-state region near 0.2 s, the peak value of the disturbance estimation error for Method 3 with $g = 0.12$ is reduced by 3.9 times compared to the case when $g = 0.03$. The disturbance estimation performance of Method 2 is similar to or little less than that of Method 3. The simulation results of the estimation error ratio are summarized in Table II. In the transient region near 0.1 s, the convergence speed of the disturbance estimation error increases as g increases. In practice, however, there is a restriction for the gain level of g due to the fast disturbance or time delay that reduces the stability margin in the frequency domain [26]. Therefore, this represents the tradeoff of gain for DDC, which needs to be considered in real implementation.

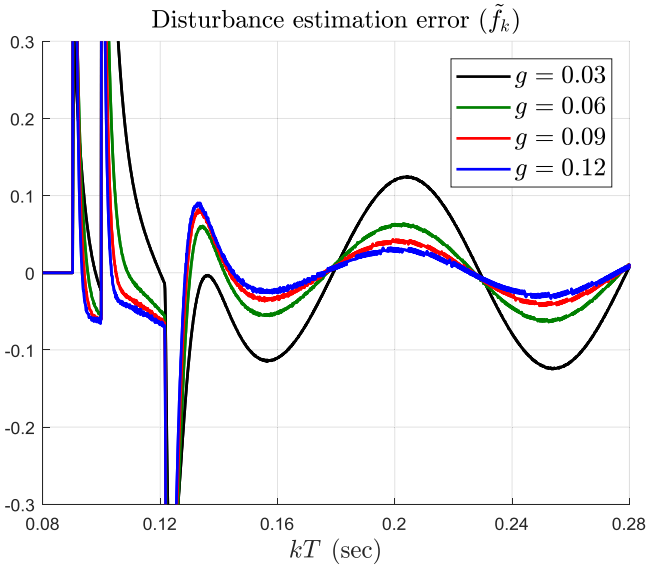

Fig. 5. Simulation results of disturbance estimation error by Method 3.

TABLE II
SIMULATION RESULTS FOR DISTURBANCE ESTIMATION ERROR IN STEADY STATE

		$g = 0.03$	$g = 0.06$	$g = 0.09$	$g = 0.12$
Peak magnitude of disturbance estimation error	Method 1	N/A	N/A	N/A	N/A
	Method 2	0.1248	0.0638	0.0429	0.0334
	Method 3	0.1246	0.0638	0.0432	0.0322

Remark 6: If we choose $\alpha = 1$, the stability of the system may not be problematic. However, the stored value of the auxiliary state does not reduce, and, thus, the error state $e_{1,k}$ will not converge to zero.

Remark 7: The design method for the selection of α depends on various applications. Fig. 6 shows the simulation results for different gains of α where the other parameters are the same as those in Table I. When α is closer to one, the auxiliary dynamics will become slower. It will lead the system (37) to be slower because α is one of the eigenvalues of (37). On the other hand, when α is selected as a smaller positive value, the auxiliary dynamics make the system to be faster, which poses the possibility of performance degradation under control saturation.

V. EXPERIMENTS

Experiments on a commercial ball-screw drive system are performed to show the effectiveness of the proposed method. The drive system consists of a 400-W ac servo motor, an incremental encoder with 2^{23} counts/revolution (RS Automation, Korea), a 400-W servo driver (RS Automation, Korea), and a ball-screw drive load which is mechanically coupled with a servo motor. The experimental setup is shown in Fig. 7, and the block diagram of the servo system is shown in Fig. 8. A second-order

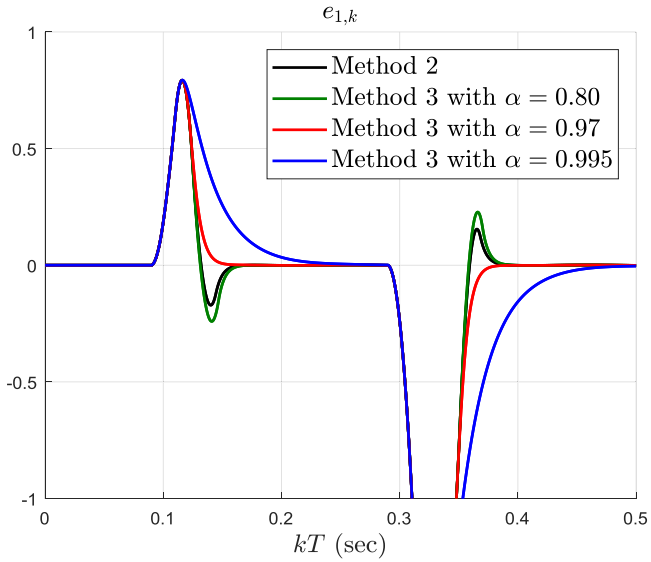

Fig. 6. Simulation results of Method 2 and Method 3 with different α.

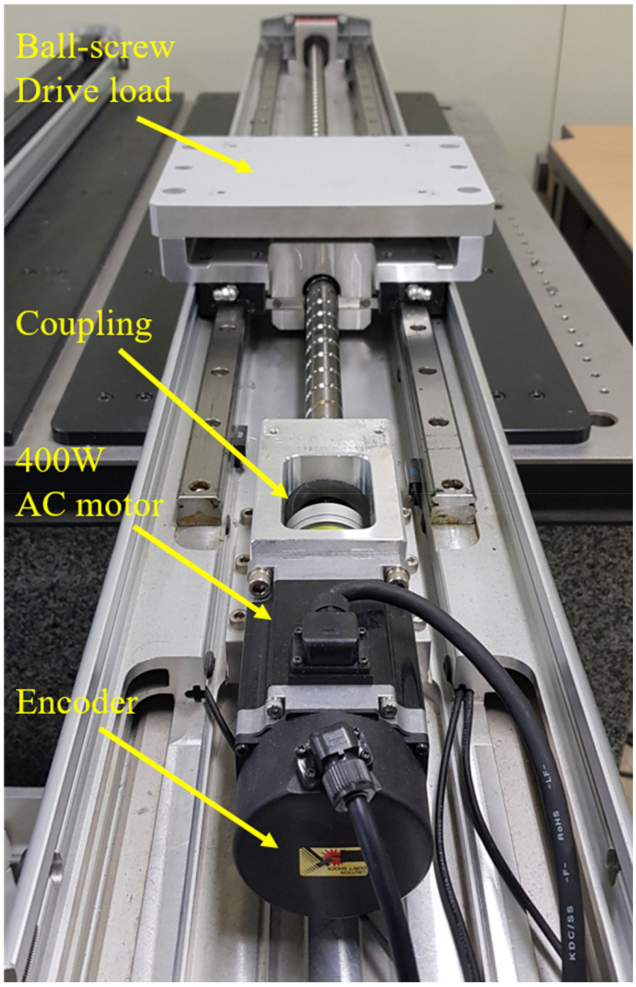

Fig. 7. Experimental setup.

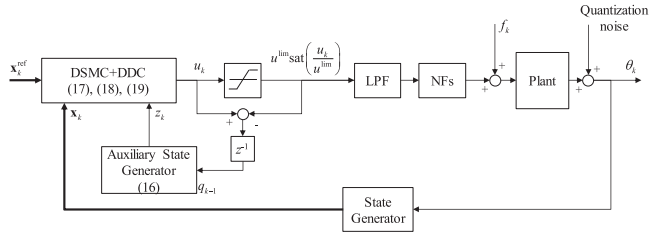

Fig. 8. Block diagram of DSMC with DDC and auxiliary state.

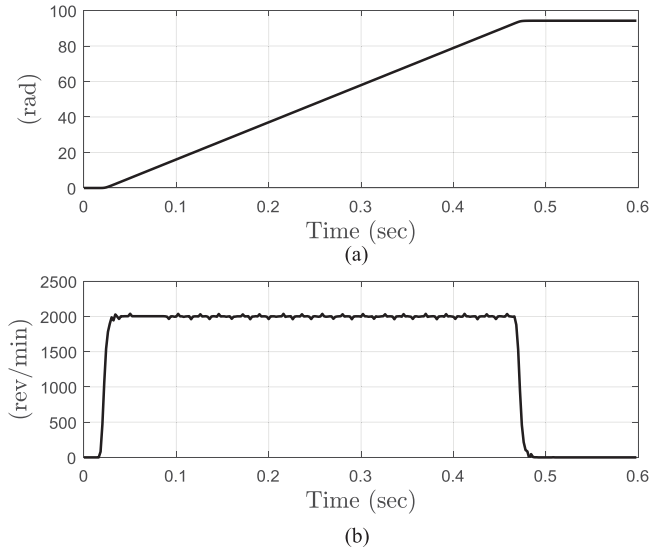

Fig. 9. Reference position and velocity. (a) Reference position. (b) Reference velocity.

Butterworth-type low-pass filter (LPF) with cutoff frequency at 2000 Hz is cascaded right after the controller to ameliorate the high-frequency noises in the measurement from the encoder. In addition, two bi-quad notch filters with center frequencies at 871 Hz and 1615 Hz are cascaded right after the LPF to suppress the high-frequency resonances in the ball-screw drive system. The resonance frequencies of the system were found by an online frequency estimator [49] in prior. By utilizing the LPF and the two NFs, the system can be modeled as follows:

$$\begin{bmatrix}\theta_{k+1}\\ \omega_{k+1}\end{bmatrix} = \begin{bmatrix}1 & T\\ 0 & 1\end{bmatrix}\begin{bmatrix}\theta_k\\ \omega_k\end{bmatrix} + \begin{bmatrix}k_t T^2/2J\\ k_t T/J\end{bmatrix}\left(u^{\lim}\mathrm{sat}\left(\frac{u_k}{u^{\lim}}\right) + f_k\right) \tag{48}$$

where θ_k and ω_k are the angular position and the angular velocity of the motor, respectively. The maximum control input $u^{\lim}$ is 5 A. The sampling period T is 0.125 ms. The torque constant k_t is $0.33\ \mathrm{N\cdot m/A}$. The total inertia J, which combines the motor inertia and the load inertia, is $2.32 \times 10^{-4}\ \mathrm{kg\cdot m^2}$. The gain parameters of the DSMC with DDC and auxiliary state are given in Table I. In this test, the desired position is 15 turns, and the desired velocity is 2000 rev/min. The acceleration and deceleration times of reference are both 5 ms. Fig. 9 shows the reference profile. The control algorithms of Methods 2 and 3 that are introduced in the simulation Section IV are implemented in the digital signal processor of the servo driver.

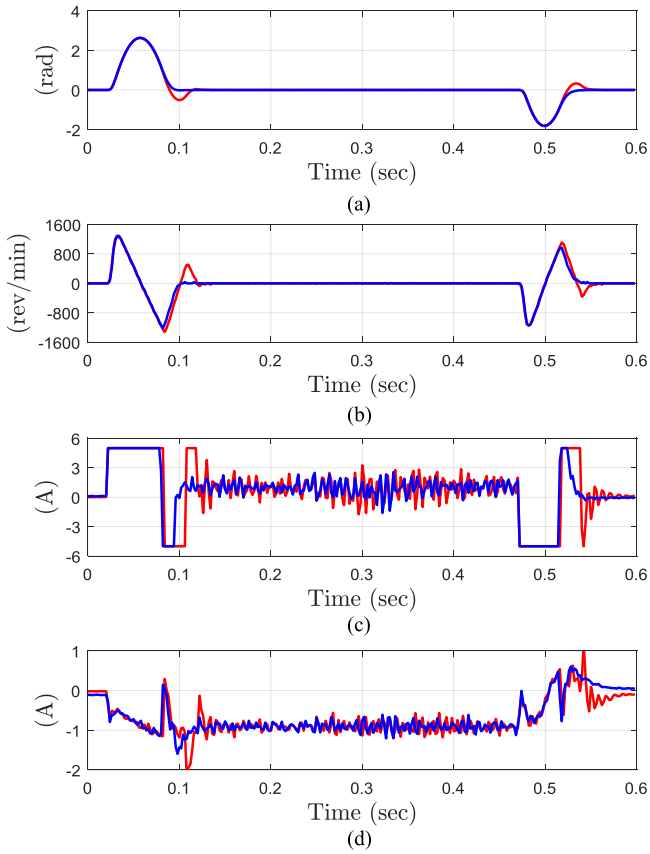

Fig. 10. Experimental results (red-line: Method 2 and blue-line: Method 3). (a) Position error. (b) Velocity error. (c) Control input. (d) Disturbance estimate ($\tilde{f}_k$).

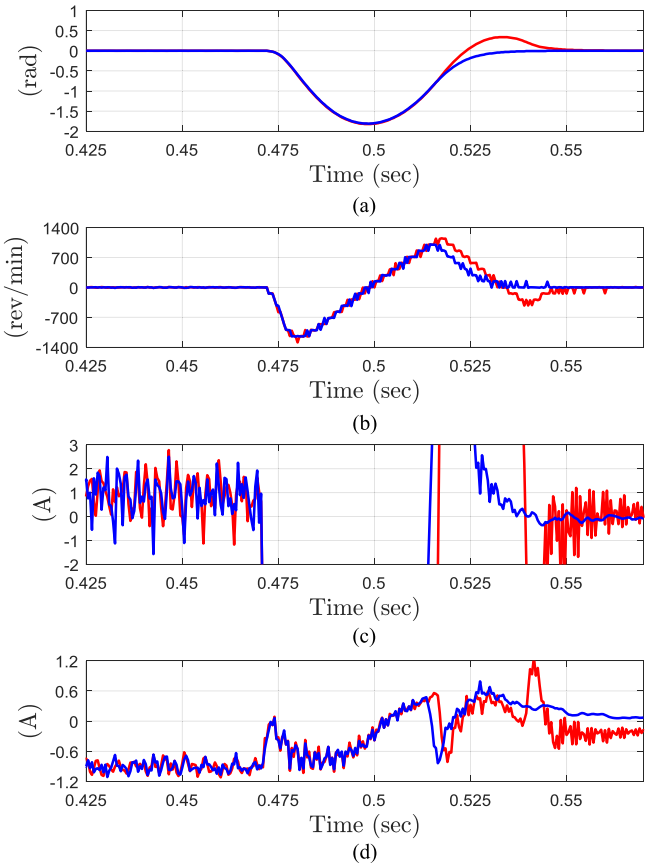

Fig. 11. Zoomed in plot of Fig. 10 (red-line: Method 2 and blue-line: Method 3). (a) Position error. (b) Velocity error. (c) Control input. (d) Disturbance estimate ($\tilde{f}_k$).

Due to the discrete-time domain representation, the proposed method can be directly implemented to the embedded systems without discretization process.

Fig. 10 shows the experimental results for Methods 2 and 3. Method 1 cannot be tested in the system due to its instability under control saturation as shown in Section IV. The zoomed-in plot of Fig. 10 is depicted in Fig. 11. In Fig. 11(a), Method 2 exhibits the second peak in the position error due to the windup effect of the switching function. On the other hand, the second peak does not occur when Method 3 is applied. The third peak of velocity error for Method 2 occurs as shown in Fig. 11(b). On the other hand, the third peak does not occur when Method 3 is applied. Method 3 has a smaller amount of time duration in control saturation compared to that of Method 2 as shown in Fig. 11(c). Chattering is significantly ameliorated because the boundary layer technique is applied in both cases. In Fig. 11(c), there are a small quantization noise in the measurement and a small vibration due to unmodelled dynamics in the ball-screw drive system, which can be further reduced by tuning the parameters of the LPF and the two NFs. The disturbance estimates for Method 2 and 3 are not completely zero because they estimate and compensate for disturbances such as frictions and model uncertainties as shown in Fig. 11(d). In consistency with the simulation results in Section IV, Method 3 provides smoother responses than Method 2, attributed to the auxiliary state. Table III summarizes the experimental results in Fig. 11. These results quantitatively show that the proposed DSMC with DDC, and auxiliary state method is highly effective under disturbances and control saturation.

TABLE III
EXPERIMENTAL RESULTS IN BALL-SCREW DRIVE SYSTEM IN FIG. 11

Measurements	Method 2	Method 3
First peak in position error (rad)	-1.8208	-1.8126
Second peak in position error (rad)	0.3375	0
First peak in velocity error (rev/min)	-1,289	-1,153
Second peak in the velocity error (rev/min)	1,150	1,010
Third peak in the velocity error (rev/min)	-106	0
Duration of control saturation (ms)	138	101

VI. CONCLUSION

This article developed a novel DSMC with DDC method to effectively compensate for disturbances and control saturation using the auxiliary state. For a constrained input system, the stability of the original DSMC with DDC was not guaranteed. On the other hand, the proposed method preserves the asymptotic convergence property of the disturbance estimation error dynamics and maintains the stability of SMC in

the presence of disturbances and control saturation. To show the effectiveness of the proposed method, simulations and experiments on an industrial ball-screw drive system were performed. Tracking performances under disturbances and control saturation were significantly improved by using the proposed method.

Acknowledgment

English proofreading service was supported by Brain Korea 21 Plus Project funded by the National Research Foundation of Korea (NRF).

References

[1] M. Basin, P. Yu, and Y. Shtessel, "Hypersonic missile adaptive sliding mode control using finite-and fixed-time observers," *IEEE Trans. Ind. Electron.*, vol. 65, no. 1, pp. 930–941, Jan. 2018.

[2] H. Li and D. Yao, "Adaptive sliding-mode control of Markov jump nonlinear systems with actuator faults," *IEEE Trans. Autom. Control*, vol. 62, no. 4, pp. 1933–1939, Apr. 2017.

[3] F. Chen, R. Jiang, K. Zhang, B. Jiang, and G. Tao, "Robust backstepping sliding-mode control and observer-based fault estimation for a quadrotor UAV," *IEEE Trans. Ind. Electron.*, vol. 63, no. 8, pp. 5044–5056, Aug. 2016.

[4] X. Zhang, L. Sun, K. Zhao, and L. Sun, "Nonlinear speed control for PMSM system using sliding-mode control and disturbance compensation techniques," *IEEE Trans. Power Electron.*, vol. 28, no. 3, pp. 1358–1365, Jul. 2013.

[5] J. Yang, S. Li, and X. Yu, "Sliding-mode control for systems with mismatched uncertainties via a disturbance observer," *IEEE Trans. Ind. Electron.*, vol. 60, no. 1, pp. 160–169, Jan. 2013.

[6] D. Ginoya, P. Shendge, and S. Phadke, "Sliding mode control for mismatched uncertain systems using an extended disturbance observer," *IEEE Trans. Ind. Electron.*, vol. 61, no. 4, pp. 1983–1992, Apr. 2014.

[7] J. Zhang, X. Liu, Y. Xia, Z. Zuo, and Y. Wang, "Disturbance observer-based integral sliding-mode control for systems with mismatched disturbances," *IEEE Trans. Ind. Electron.*, vol. 63, no. 11, pp. 7040–7048, Nov. 2016.

[8] N. Wang, S. Su, X. Pan, X. Yu, and G. Xie, "Yaw-guided trajectory tracking control of an asymmetric underactuated surface vehicle," *IEEE Trans. Ind. Informat.*, vol. 15, no. 6, pp. 3502–3513, Jun. 2019.

[9] N. Wang, S. Lv, W. Zhang, Z. Liu, and M. Er, "Finite-time observer based accurate tracking control of a marine vehicle with complex unknowns," *Ocean Eng*., vol. 145, pp. 406–415, Nov. 2017.

[10] L. Derafa, A. Benallegue, and L. Fridman, "Super twisting control algorithm for the attitude tracking of a four rotors UAV," *J. Franklin Inst.*, vol. 349, no. 2, pp. 685–699, Mar. 2012.

[11] A. Chalanga, S. Kamal, L. M. Fridman, B. Bandyopadhyay, and J. A. Moreno, "Implementation of super-twisting control: Super-twisting and higher order sliding-mode observer-based approaches," *IEEE Trans. Ind. Electron.*, vol. 63, no. 6, pp. 3677–3685, Jun. 2016.

[12] J. Liu, S. Vazquez, L. Wu, A. Marquez, H. Gao, and L. G. Franquelo, "Extended state observer-based sliding-mode control for three-phase power converters," *IEEE Trans. Ind. Electron.*, vol. 64, no. 1, pp. 22–31, Jan. 2017.

[13] H. Oza and S. Spurgeon, "Novel environment for the practical implementation of higher order sliding mode controllers," in *Proc. 52nd IEEE Conf. Decis. Control*, Dec. 2013, pp. 4254–4259.

[14] A. Mironova, P. Mercorelli, and A. Zedler, "A multi input sliding mode control for peltier cells using a cold–hot sliding surface," *J. Frankl. Inst.*, vol. 355, no. 18, pp. 9351–9373, Dec. 2018.

[15] J. Lee, P. H. Chang, and M. Jin, "Adaptive integral sliding mode control with time-delay estimation for robot manipulators," *IEEE Trans. Ind. Electron.*, vol. 64, no. 8, pp. 6796–6804, Aug. 2017.

[16] X. Xiang, C. Liu, H. Su, and Q. Zhang, "On decentralized adaptive full-order sliding mode control of multiple UAVs," *ISA Trans*., vol. 71, no. 2, pp. 196–205, Nov. 2017.

[17] Y. Lee, S. H. Kim, and C. C. Chung, "Integral sliding mode control with a disturbance observer for next-generation servo track writing," *Mechatronics*, vol. 40, pp. 106–114, Dec. 2016.

[18] J. Li, Q. Zhang, X. Yan, and S. Spurgeon, "Robust stabilization of T–S fuzzy stochastic descriptor systems via integral sliding modes," *IEEE Trans. Cybern.*, vol. 48, no. 9, pp. 2736–2749, Sep. 2018.

[19] Y. Wei, J. Park, J. Qiu, L. Wu, and H. Jung, "Sliding mode control for semi-Markovian jump systems via output feedback," *Automatica*, vol. 81, pp. 133–141, Jul. 2017.

[20] B. Jiang, Y. Kao, C. Gao, and X. Yao, "Passification of uncertain singular semi-Markovian jump systems with actuator failures via sliding mode approach," *IEEE Trans. Autom. Control*, vol. 62, no. 8, pp. 4138–4143, Aug. 2017.

[21] B. Jiang, H. R. Karimi, Y. Kao, and C. Gao, "A novel robust fuzzy integral sliding mode control for nonlinear semi-Markovian jump T–S fuzzy systems," *IEEE Trans. Fuzzy Syst.*, vol. 26, no. 6, pp. 3594–3604, Dec. 2018.

[22] W. Gao, Y. Wang, and A. Homaifa, "Discrete-time variable structure control systems," *IEEE Trans. Ind. Electron.*, vol. 42, no. 2, pp. 117–122, Apr. 1995.

[23] H. Ma, J. Wu, and Z. Xiong, "Discrete-time sliding-mode control with improved quasi-sliding-mode domain," *IEEE Trans. Ind. Electron.*, vol. 63, no. 10, pp. 6292–6304, Oct. 2016.

[24] Y. Eun, K. Kim, J. Kim, and D. Cho, "Discrete-time variable structure controller with a decoupled disturbance compensator and its application to a CNC servomechanism," *IEEE Trans. Control Sys. Technol.*, vol. 7, no. 4, pp. 414–423, Jul. 1999.

[25] K. Zhang, H. Su, K. Zhuang, and J. Chu, "Comments on 'Discrete-time variable structure controller with a decoupled disturbance compensator and its application to a CNC servomechanism," *IEEE Trans. Control Syst. Technol.*, vol. 11, no. 1, pp. 156–157, Jan. 2003.

[26] J. Han *et al.*, "Frequency-domain design method of discrete-time sliding mode control with generalized decoupled disturbance compensator for industrial servo systems," in *Proc. 12th IFAC Symp. Robot Control*, Aug. 2018, pp. 27–30.

[27] W. Bahn, S. Lee, S. Lee, and D. Cho, "Control of 400 watt belt-drive and 400 watt ball-screw servo systems using discrete-time variable structure control," in *Proc. 19th World Congr. Int. Fed. Autom. Control*, Aug. 2014, pp. 8378–8383.

[28] C. Milosavljevic, B. Perunicic-Drazenovic, and B. Veselic, "Discrete-time velocity servo system design using sliding mode control approach with disturbance compensation," *IEEE Trans. Ind. Informat.*, vol. 9, no. 2, pp. 920–927, May 2013.

[29] L. Ma, D. Zhao, and S. Spurgeon, "Disturbance observer based discrete time sliding mode control for a continuous stirred tank reactor," in *Proc. 15th Int. Workshop Variable Structure Syst.*, Jul. 2018, pp. 372–377.

[30] Z. Zhu, Y. Xia, and M. Fu, "Adaptive sliding mode control for attitude stabilization with actuator saturation," *IEEE Trans. Ind. Electron.*, vol. 58, no. 10, pp. 4898–4907, Oct. 2011.

[31] N. Wang, S. Su, M. Han, and W. Chen, "Backpropagating constraints-based trajectory tracking control of a quadrotor with constrained actuator dynamics and complex unknowns," *IEEE Trans. Syst., Man, Cybern. B, Cybern, Syst.*, vol. 49, no. 7, pp. 1322–1337, Jul. 2019.

[32] M. Massimetti, L. Zaccarian, T. Hu, and A. Teel, "LMI-based linear anti-windup for discrete time linear control systems," in *Proc. 45th IEEE Conf. Decis. Control*, Dec. 2006, pp. 6173–6178.

[33] G. Grimm, J. Hatfield, I. Postlethwaite, A. Teel, M. Turner, and L. Zaccarian, "Antiwindup for stable linear systems with input saturation: An LMI-based synthesis," *IEEE Trans. Autom. Control*, vol. 48, no. 9, pp. 1509–1525, Sep. 2003.

[34] A. Syaichu-Rohman and R. Middleton, "Anti-windup schemes for discrete time systems: An LMI-based design," in *Proc. 5th Asian Control Conf.*, Jul. 2004, vol. 1, pp. 554–561.

[35] Z. Zheng and M. Feroskhan, "Path following of a surface vessel with prescribed performance in the presence of input saturation and external disturbances," *IEEE/ASME Trans. Mechatron.*, vol. 22, no. 6, pp. 2564–2575, Dec. 2017.

[36] L. Sun and Z. Zheng, "Disturbance-observer-based robust backstepping attitude stabilization of spacecraft under input saturation and measurement uncertainty," *IEEE Trans. Ind. Electron.*, vol. 64, no. 10, pp. 7994–8002, Oct. 2017.

[37] L. Sun, W. Huo, and Z. Jiao, "Disturbance observer-based robust relative pose control for spacecraft rendezvous and proximity operations under input saturation," *IEEE Trans. Aerosp. Electron. Syst.*, vol. 54, no. 4, pp. 1605–1617, Aug. 2018.

[38] L. Sun, W. Huo, and Z. Jiao, "Adaptive backstepping control of spacecraft rendezvous and proximity operations with input saturation and full-state constraint," *IEEE Trans. Ind. Electron.*, vol. 64, no. 1, pp. 480–492, Jan. 2017.

[39] R. Cui, X. Zhang, and D. Cui, "Adaptive sliding-mode attitude control for autonomous underwater vehicles with input nonlinearities," *Ocean Eng.*, vol. 123, no. 1, pp. 45–54, Sep. 2016.
[40] J. Han *et al.*, "Decoupled disturbance compensation under control saturation with discrete-time variable structure control method in industrial servo systems," in *Proc. 16th Int. Conf. Control, Autom. Syst.*, Oct. 2016, pp. 16–19.
[41] B. Zhou, G. Duan, and Z. Lin, "Global stabilization of the double integrator system with saturation and delay in the input," *Circuits Syst. I, Reg. Papers*, vol. 57, no. 6, pp. 1371–1383, Jun. 2010.
[42] Y. Dong and J. Huang, "A leader–following rendezvous problem of double integrator multi-agent systems," *Automatica*, vol. 49, no. 5, pp. 1386–1391, May 2013.
[43] B. Zhu, K. Guo, and L. Xie, "A new distributed model predictive control for unconstrained double-integrator multi-agent systems," *IEEE Trans. Autom. Control*, vol. 63, no. 12, pp. 4367–4374, Dec. 2018.
[44] D. Palma, F. Arrichiello, G. Parlangeli, and G. Indiveri, "Underwater localization using single beacon measurements: Observability analysis for a double integrator system," *Ocean Eng.*, vol. 142, no. 15, pp. 650–665, Sep. 2017.
[45] Z. Jiang and Y. Wang, "A converse Lyapunov theorem for discrete-time systems with disturbances," *Syst. Control Lett.*, vol. 45, no. 1, pp. 49–58, Jan. 2002.
[46] M. C. Pai, "Discrete-time sliding mode control for robust tracking and model following of systems with state and input delays," *Nonlinear Dyn.*, vol. 76, no. 3, pp. 1769–1779, May 2014.
[47] S. Mobayen, "An LMI-based robust tracker for uncertain linear systems with multiple time-varying delays using optimal composite nonlinear feedback technique," *Nonlinear Dyn.*, vol. 80, no. 1–2, pp. 917–927, Apr. 2015.
[48] S. P. Boyd, L. El Ghaoui, E. Feron, and V. Balakrishnan, *Linear Matrix Inequalities in System and Control Theory*. Philadelphia, PA, USA: SIAM, 1994.
[49] W. Bahn, T. Kim, S. Lee, and D. Cho, "Resonant frequency estimation for adaptive notch filters in industrial servo systems," *Mechatronics*, vol. 41, pp. 45–57, Feb. 2017.
[50] Y. Wei, J. Qiu, and H. K. Lam, "A novel approach to reliable output feedback control of fuzzy-affine systems with time delays and sensor faults," *IEEE Trans. Fuzzy Syst.*, vol. 25, no. 6, pp. 1808–1823, Dec. 2017.
[51] Y. Wei, J. Qiu, and H. R. Karimi, "Fuzzy-affine-model-based memory filter design of nonlinear systems with time-varying delay," *IEEE Trans. Fuzzy Syst.*, vol. 26, no. 2, pp. 504–517, Apr. 2018.

Ji-Seok Han (S'18) received the B.S. degree in electrical and electronics engineering from Chung-Ang University, Seoul, Korea, in 2015. He is currently working toward the Ph.D. degree at the Department of Electrical and Computer Engineering, Seoul National University, Seoul.

His research interests include applications of nonlinear control theory to servo drive and sensors for motion control applications.

Tae-Il Kim received the B.S. and M.S. degrees in electrical and computer engineering from Seoul National University, Seoul, Korea, in 2010 and 2012, respectively. He is currently working toward the Ph.D. degree with the Department of Electrical and Computer Engineering, Seoul National University, Seoul.

He was a Research Engineer with Samsung Techwin from 2012 to 2015. His research interests include applications of nonlinear control theory to servo drive and sensors for motion control applications.

Tae-Ho Oh received the B.S. degree in electrical and computer engineering from Seoul National University, Seoul, Korea, in 2017. He is currently working toward the Ph.D. degree with the Department of Electrical and Computer Engineering, Seoul National University.

His research interests include applications of nonlinear control theory and machine learning algorithms to servo drive and sensors.

Sang-Hoon Lee received the B.S., M.S. and Ph.D. degrees in electrical and computer engineering from Seoul National University, Seoul, Korea, in 1991, 1993 and 1997, respectively.

He is currently a Research and Development Center Manager with RS Automation Company, Ltd., Pyeongtaek, Korea. His current research interests include nonlinear control theory and its application to electric machines and factory automation.

Dong-Il "Dan" Cho (M'88) received the B.S. degree from Carnegie-Mellon University, Pittsburgh, PA, USA, in 1980, and the M.S. and Ph.D. degrees from the Massachusetts Institute of Technology, Cambridge, MA, USA, in 1984 and 1988, respectively, all in mechnanical engineering.

From 1987 to 1993, he was an Assistant Professor with Princeton University, Princeton, NJ, USA. Since 1993, he has been with the Department of Electrical and Computer Engineering, Seoul National University, Seoul, Korea, where he is currently a Professor. He has authored/coauthored more than 130 international journal articles, and is holder/coholder of 120 U.S. and Korean patents.

Dr. Cho has served on the editorial board of many international journals. He currently is the Senior Editor for IEEE JOURNAL OF MICROELECTROMECHANICAL SYSTEMS and the Senior Editor for *Mechatronics*. He was the President of ICROS and BOG Member of IEEE CSS, and is currently the Vice President of IFAC, Chair of the Technical Board of IFAC, and AdCom Member of IEEE EDS. He is an elected Senior Member of National Academy of Engineering of Korea.